An Insight: Studies of Atomic and Molecular Adsorption on Co(0001)

Karin Habermehl-Cwirzen

Laboratory of Physics
Helsinki University of Technology
FIN-02015 HUT, Finland

Abstract

This thesis deals with the adsorption of selected atoms and molecules on a well defined single crystal cobalt surface. X-ray photoelectron spectroscopy has been used to identify different adsorption sites and coverages. Work function measurements have been utilized to monitor the strength of the interaction between adsorbed species and cobalt substrate. Thermal desorption spectroscopy has identified the desorption products and has given information on the activation energies for desorption. By means of low energy electron diffraction measurements the adsorbate unit cell and, by utilizing I-V curve analysis, the atomic positions have been determined.

Adsorption processes are important, e.g. in catalytic reactions, therefore studying adsorption and desorption of atoms and molecules on a well-defined surface can give useful insight information on reactions and how these reactions might be influenced.

We have studied a selection of important atoms and molecules on a Co(0001) surface. Deuterium has been extensively studied as single adsorbate as well as in coadsorption with carbon monoxide and sulfur. Methanol adsorption and O-H bond scission has been an important topic of this thesis. Benzene adsorption has been determined at length, as a single component including I-V curve analysis and DFT calculations, as well as coadsorbed with carbon monoxide. Sulfur, a common unwanted component in a variety of processes like, e.g. crude oil refinery, was investigated as single adsorbate as well as coadsorbed with carbon monoxide.

Acknowledgement

The experimental part of this thesis has been done in the Laboratory of Physics at the Helsinki University of Technology almost exclusively during April 1999-November 2003.

At first, I want to say thanks to Prof. Pekka Hautojärvi, who enabled me to come to Finland and work in his laboratory. I also want to express my gratitude towards Dr. Jouko Lahtinen. Both gave me a quite flexible research task, in which I was able to incorporate my own ideas.

Special thanks I have to give to Jukka Vaari and Teuvo Vaara (I will mix up your names forever) for bequeath such a well-prepared cobalt sample to me. Thanks also to my colleges in the surface science group: TkL Kalle Kauraala for helping to get accustomed to the equipment. Mikko Aroniemi, with whom I can discuss everyday problems even in German, as well as Jani Sainio, Jukka Katainen and Mårten Ericson. I will never ever forget the day when Mårten called to Denmark, initially speaking Swedish but after two sentences switching to English. Thanks to my summer students and students in my Physics lab. They showed me, that being an assistant is not always as easy as I thought initially.

Big thanks to Dr. Karen Johnston, my office mate for the last few months. I enjoyed our conversations about "DFT and other things". I will miss our common morning coffee.

Thanks to all the people in the Lab. At this point I want to mention just a few names, which stand for the others. Eija Järvinen, who lent me a sympathetic ear for all kind of problems with bureaucratic papers. Eero Turtianen, who spoke with me Finnish, and was always helpful with refilling liquid nitrogen.

I also want to acknowledge the funding of my research by the Academy of Finland. Financing was done by the National Graduate School in Materials Physics as well as research project funding.

Special thanks to my family for their continual support, for being there, for listening, for encouraging and loving: my parents, my brother and last but not least my husband Andrzej and our little daughter Emily. You are the most important people in my life. ILY!

List of Publications

This thesis consists of this overview and the following publications:

I.   K.M.E. Habermehl-Cwirzen, K.Kauraala and J. Lahtinen, Hydrogen on Cobalt: The Effects of Carbon Monoxide and Sulphur Additives on the D_2/Co(0001) System, Physica Scripta. Vol T108, 28-32, 2004

II.   K. Habermehl-Cwirzen, J. Lahtinen and P. Hautojärvi, Methanol on Co(0001): XPS, TDS, WF and LEED results, Surf. Sci. 598 (2005) 128-135

III.   K.M.E. Habermehl-Cwirzen, J. Katainen, J. Lahtinen and P. Hautojärvi, An experimental study on adsorption of benzene on Co(0001), Surf. Sci. 507-510 (2002) 57-61

IV.   K. Pussi, M. Lindroos, J. Katainen, K.Habermehl-Cwirzen, J. Lahtinen and A.P. Seitsonen, The ($\sqrt{7}$ x $\sqrt{7}$)R19.1°-C_6H_6 adsorption structure on Co(0001): a combined Tensor Leed and DFT study, Surf. Sci. 572 (2004) 1-10

V.   K. Habermehl-Cwirzen, J. Lahtinen and P. Hautojärvi, Coadsorption of CO and C_6H_6 on Co(0001), Surf. Sci. 584 (2005) 70-76

VI.   K. Habermehl-Cwirzen and J. Lahtinen, Sulfur poisoning of the CO adsorption on Co(0001), Surf. Sci. 573 (2004) 183-190

VII.   J. Lahtinen, P. Kantola, S. Jaatinen, K. Habermehl-Cwirzen and P. Salo, LEED and DFT Investigation on the (2 x 2)-S Overlayer on Co(0001), Surf. Sci. 599 (2005) 113-121

The author's contribution

The author has had an active role in all stages of the work reported in this thesis. She has participated in the planning and performing of the experiments reported in the publications I, III, IV and VII. She has planned and performed all the experiments in publications II, V and VI. She has analyzed the experimental data and largely contributed to the interpretation of the results reported in publications I-III and V-VI. The author has written publications I – III and V-VI and contributed to the writing of publications IV and VII.

Table of Contents

Publications

1 Introduction

This thesis focuses on the adsorption of selected atoms and molecules on cobalt. These systems are thought to serve as models for more complex catalytic reactions on cobalt-based catalysts.

The element cobalt was discovered in 1735 by the Swedish chemist Georg Brandt. The name cobalt has its origin in the German miners language: Ores, which looked metallic but did not contain the anticipated metal but instead produced highly toxic fumes (As_4O_6) were called in former times "Kobold", meaning a ghost or evil spirit living in the forest and mines, who teases miners. [1,2]. These days cobalt is used for instance in cobalt-based alloys in mechanical engineering, e.g. in jet engines, but also as pigment for glass, metals and enamel. Moreover, cobalt is a frequently incorporated element in industrial catalysts.

Catalysts increase the conversion velocity and can improve the selectivity of reactions. Catalysts are an important world market segment [3]. In 2005 a turnover of 11.5 billion US dollars on the world wide catalyst market is expected. Nowadays one important catalytic market share is environmental catalysis. The reduction of pollutants to meet the strict legal constraints - especially strict threshold values for sulfur and aromatics have to be abided - is the reason for the enormous growth in this sector. The implication of sulfur as well as benzene was one reason for our research on these substances [publications I, III and IV].

Another catalytic market segment is stimulated by the ongoing rise in crude oil prices and the limited reserves of crude oil: the gas-to-liquid technology [4]. Natural gas consists of methane, other hydrocarbons, water vapor, hydrogen sulfide and other compounds. After separating the methane from the other hydrocarbons, methane is first transformed to synthesis gas - consisting of hydrogen and carbon monoxide - and as a second step carbon monoxide is hydrogenated to clean gasoline or methanol. Methanol adsorption and reaction on cobalt was the objective of publication II.

For the development of industrially successful catalysts, the determination of catalytic reaction mechanisms is useful. By knowing the single reaction steps and

understanding how these steps can be influenced low-priced, selective and efficient catalysts can more easily be developed.

The problem with industrial catalysts is that the system is so complex that obtaining reliable data on molecular level is difficult or impossible. Therefore model systems like single crystals in a well defined environment are used. Pressure and temperature restrictions have their origin in the used methods and in the requirements for the cleanliness of the sample.

Nevertheless it has to be kept in mind that results in surface science can not be directly extrapolated to predict the behavior of industrial catalysts. The keywords are here "material gap", "pressure gap" and "temperature gap". In our research the sample is a single crystal in a UHV (ultra high vacuum) environment with adsorption temperatures of about 160K-320K. Whereas a typical industrial catalyst consists of several elements supported on a substrate and exposed to a pressure range about 10^{13} times higher than in our UHV system. Additionally, reactions in an industrial reactor usually take place at elevated temperatures.

In surface science we deal with a great variety of experimental methods, each of them offering a piece of information on the surface and surface processes. Like pieces of a puzzle they have to be put together correctly to obtain the general view. One technique alone cannot offer all information. With our equipment it is possible to perform XPS, TDS and LEED measurements. XPS (X-ray photoelectron spectroscopy) gives information on the chemical composition and local adsorption site. Additionally XPS was applied in this thesis to follow the change in the work function. TDS (thermal desorption spectroscopy) was used to attain an insight on the bonding strength of the adsorbates and their decomposition products. LEED (low energy electron diffraction) patterns were analyzed in two ways. In qualitative LEED, the diffraction pattern can be used to obtain information on the unit cell of the adsorbate and the sample surface. The coverage can be possibly extracted from the geometry of the pattern itself, too. In quantitative LEED, analyzing the LEED spot intensity leads - with the help of elaborate computer modeling - to the exact adsorption position of the atoms.

This thesis deals with the adsorption of single species atoms/molecules as well as cases of coadsorption on a Co(0001) substrate. Deuterium adsorption was studied

mainly by LEED and TDS. Deuterium is not directly accessible by XPS but the influence of deuterium on the work function could be successfully studied with the help of photoelectron spectroscopy [publication I]. The dissociative behavior of methanol on cobalt is the topic of publication II. Our study serves as a basis for the usage of cobalt-based catalysts in fuel cells and other engine types using methanol. The adsorption of benzene is dealt with in publications III and IV. Benzene was chosen as a model for more complicated aromatic hydrocarbons. Publication VII deals with the adsorption properties of sulfur. Sulfur is a commonly unwanted component in crude oil and therefore desulphurization is an important process in the oil-processing industry. The influence of coadsoption of carbon monoxide or sulfur with deuterium has been published in publication I. The interaction of sulfur and carbon monoxide on each other is shown in publication VI. Coadsorption of benzene and carbon monoxide as an example of a presumed electron donator / electron acceptor system is studied in publication V.

2 Experimental Methods and Set-up

2.1 UHV chamber and Equipment

To investigate surfaces and adsorption structures, UHV is desirable as UHV guarantees that the sample stays reasonably uncontaminated by background gas during the measurements. This applies especially to cases where a clean or only partially covered reactive surface is used.

For obtaining the rough pressure after opening the chamber a Leybold-Heraeus Turbovac 150l/s turbo pump was used, which was in a later stage exchanged to a Varian turbo pump. The turbo pump was also active during the sputtering of the sample. The UHV pressure was sustained by a Varian Star Cell VacIon 400l/s ion pump and a titanium sublimation pump.

The experimental set-up contained facilities for LEED, XPS and TDS measurements. The set-up can be seen in the schematic view shown in fig. 1 [5].
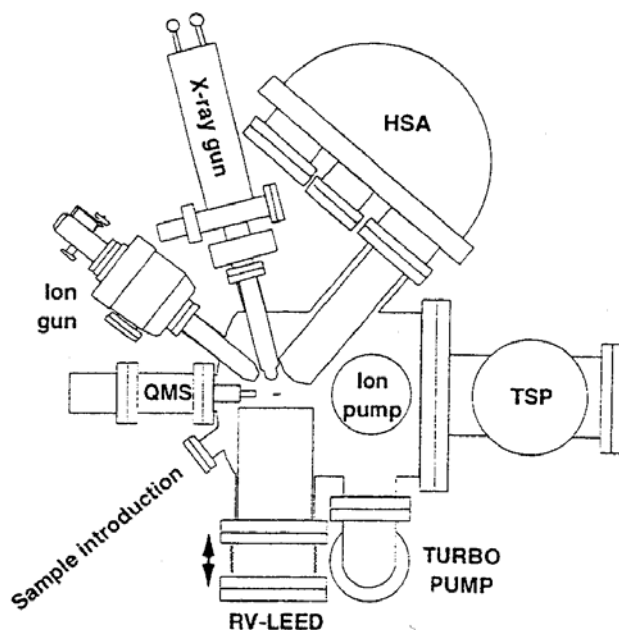

Fig.1: Schematic drawing of the UHV apparatus [5]. The apparatus is equipped with several pumps i.e. (TSP) titanium sublimation pump, ion pump and turbo pump. The sample can be investigated by (RV-LEED) rear view LEED. The X-ray gun produces the photons for the XPS. The photoelectrons are analyzed with the help of the (HSA) hemispherical analyzer. The (QMS) quadrupole mass spectrometer serves as a analyzer for the desorbing species during TDS measurements.

2.2 Sample and Sample Preparation

As sample a disc-shaped Co(0001) single crystal was used throughout the measurements. The crystal - with 99.999% purity - was originally purchased from Metal Crystals and Oxides Ltd. The crystal sample has a diameter of 11mm and a thickness of about 1mm. It was mounted to the sample holder by spot-welded tantalum wires, which were also used for conducting the heating current to the sample [fig.2].

The initial cleaning consisted of repeated sputtering - with 3keV Ar^+-ions - and subsequent annealing cycles to remove all initial contaminants like N, O, Cl and C. The basic preparation of the crystal had been done by J. Vaari during his doctorate [5]. The initial cleaning left the cobalt crystal in such a good cleanliness, that a short preparation process before each measurement was enough to obtain a clean cobalt surface. This process consisted of sputtering with 1keV Ar^+-ions for about 1h at room temperature, followed by a continuation of sputtering while heating the sample to about 600K. After 20 min the sputtering process was stopped and the sample further annealed for additional 20 min at about 640K. The cleanliness was verified by XPS and additionally by occasional LEED measurements.
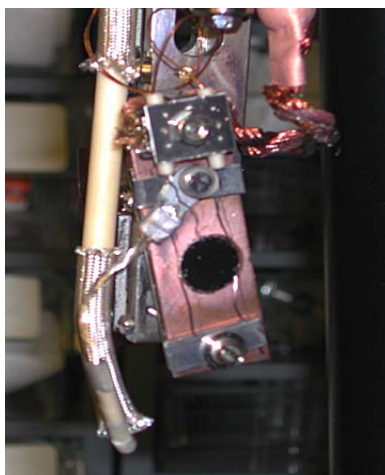

Fig.2: Cobalt sample used in our measurements.

During LEED measurements a negative bias voltage was applied to the sample during parameter adjustment, to ensure a minimum of radiation damage to the surface. At each step two pictures were taken and averaged to increase the signal to noise ratio. These pictures were analyzed off-line after the measurement series. The sample was

biased with a voltage of -25eV during XPS measurements to ensure that the photoelectron signal originated from the sample only. With this measure contributions from, e.g. the sample holder or wiring, could be excluded.

2.3 TDS (Thermal Desorption Spectroscopy)

TDS is a simple and straightforward surface science technique. First, the sample surface is exposed to a certain gas to adsorb gas atoms or molecules. During conduction of a TDS experiment the temperature is raised slowly and linearly. Several processes can take place including diffusion of the adsorbate into the bulk or a reaction between adsorbate and substrate to form a surface compound. One other possibility - which is used for TDS - is that with increasing temperature the adsorbed molecules or atoms leave the surface in order of the bond strength. The surface concentration decreases with increasing substrate temperature until the surface is clean, unless there is a re-adsorption from the gas phase taking place [6-8]. The final temperature should be chosen so that it is high enough to desorb all the adsorbed molecules / atoms, but not so high that it damages the sample, e.g. by phase transformation. In our study the temperature was limited by the phase transformation of cobalt at 694K. Above that temperature the allotrope fcc structure of cobalt is more stable and a non-reversible phase transformation from hcp to fcc takes place [2].

The desorbed species are being analyzed with a mass spectrometer. In our laboratory a Balzers QMG 420 quadrupole mass spectrometer is used. The data from a TDS measurement consist of the number of mass-to-charge-ratio fragments versus time. By knowing the heating rate, the time scale can be then transformed to a temperature scale.

TDS spectra deliver following information [6]:
- The area under the peak is proportional to the amount of originally adsorbed molecules/ atoms, if the pumping speed is high enough to ensure that no re-adsorption takes place. From this data it is then possible to calculate the initial coverage.
- Desorption kinetics can be obtained from the peak profile.

- The amount of different adsorption sites.
- The population of each adsorption site.
- Possible adsorbate interaction.
- The position of the peak is related to the desorption activation energy. The higher the peak maximum temperature the stronger is the molecule / atom adsorbed.

Kinetic values, e.g. the activation energy, can be calculated from the results of the TDS measurements, too [9-13]. The desorption process can be formally described by the following equation:

$$r_d = -v_n \; \theta^n \; e^{\left(\dfrac{-E_{a,des}}{RT} \right)}. \qquad\qquad (1)$$

r_d: desorption rate   R: gas constant ($8.31451 \; J \; K^{-1} \; mol^{-1}$)

v_n: pre-exponential factor   T: peak maximum temperature (in K)

θ: total coverage   n: reaction order

$E_{a,des}$: activation energy for desorption of species A

Both the pre-exponential factor as well as the activation energy for desorption are generally considered to be dependent on the coverage.

2.4 XPS (X-ray Photoelectron Spectroscopy)

The photoelectric effect was first observed by Hertz in 1887 and was later explained by Einstein in 1905: when a photon transfers its energy to an electron, the photon is annihilated and the electron transferred in an excited state. On the basis of this effect Kai Siegbahn and his research group in Uppsala / Sweden developed XPS or ESCA, Electron Spectroscopy for Chemical Analysis, as they called it. For his work Kai Siegbahn received the Nobel Prize in Physics in 1981.

Our apparatus contains a dual aluminum / magnesium anode as photon source. Aluminum is having the K_α line at 1486.6eV and magnesium its K_α line at 1253.6eV. The X-ray line width is about 1eV (Al K_α: 0.85eV and Mg K_α: 0.7eV) for these materials

[14]. X-rays penetrate deep into the material and excite photoelectrons on their way. Due to inelastic scattering of these electrons and therewith loss of energy, XPS is a very surface sensitive method.

XPS makes use of the photoelectric effect. The ionization process can be approximately described by the one-atom model: When an X-ray is absorbed by an atom the total energy of the system comprises of the photon energy hv and the energy of the atom in the initial state E_i. If then a photoelectron is ejected, the total energy comprises of the kinetic energy of the photoelectron E_{kin} and the final state energy of the ion E_f:

$$hv + E_i = E_{kin} + E_f. \tag{2}$$

The difference between E_f and E_i is the binding energy E_b. E_b can be easily determined as the X-ray energy hv is known and E_{kin} can be measured by means of an electron energy analyzer.

In practice, the binding energy term has to be split in two terms, the actual binding energy referred to the Fermi level E_B and the work function of the sample surface Φ (minimum energy to bring an electron from the Fermi level just outside the sample surface):

$$hv = E_{kin} + E_B + \Phi_{sample.} \tag{3}$$

An electron energy analyzer is used to measure the kinetic energy of the photoelectron. This complicates equation (3), as the work functions of the analyzer material and the sample material are usually not the same. This difference in the work functions leads to an altered kinetic energy E^*_{kin} which is the kinetic energy as determined by the energy analyzer.

$$E_B = hv - E^*_{kin} - \Phi_{analyzer}. \tag{4}$$

The kinetic energy of the photoelectrons is analyzed with a hemispherical electron analyzer and afterwards presented in a spectrum as intensity versus binding energy. This spectrum shows peaks, which represent the binding energy of this photoelectron.

Each element has a unique set of binding energies and therefore the elemental composition of the surface can be determined. From the binding energy you can find out following facts about the sample:

- The elements it is made of.
- The relative quantity of each element.
- The chemical state of the elements.

Detailed information from the XP spectrum is obtained by first fitting a background function to the peak tails. This background is removed by subtraction from the spectrum. Subsequently the remaining signal is peak fitted with single or multiple peaks. The peaks are fitted by choosing the initial values for the fit, such as the number of peaks, peak type and approximate peak heights, peak positions and peak width. These data are used as an approximate base for the fitting routine. The fitting procedure is iterated until the calculations give a reliable result. The peak intensity, which is the area under the fitted peak, is proportional to the atomic concentration in the measurement area [11-12, 14].

2.5 LEED (Low Energy Electron Diffraction)

Broken equipment can even lead to the Nobel Prize, as the case of Clinton Davisson shows. In 1925 he and Lester Germer worked on elastic scattering of electrons at a polycrystal of nickel. After the broken vacuum trap was repaired and the crystal at very high temperatures annealed, they were surprised by their results showing an angular distribution of scattered electrons. Opening the equipment again and investigating the crystal revealed that the polycrystalline nickel had transformed into a single crystal. In 1926 after meeting leading physicists during a trip to England, Davisson realized that their "failed" experiment was actually the result of electron diffraction at the single crystal surface – the first time someone had shown experimentally the wave nature of electrons. The first paper on this topic was published by Germer and Davidsson in 1927. In 1937 Davisson and G.P. Thomson got the Nobel Prize in Physics.

In LEED electrons with energies between 20-200eV impinge on the sample surface, where they are backscattered. This energy range corresponds to an electron wavelength of about 0.1-3Å and is the same order of magnitude as the atomic distances in solids. These low energy electrons have a short mean free path in solids and are therefore surface sensitive.

The backscattered electrons are filtered by a set of retarding grids, which selects the elastically scattered electrons. These electrons are then accelerated onto a fluorescent screen. The screen glow intensity is proportional to the incident electron flux [15].

As the diffraction pattern is an image of the reciprocal lattice, some calculations have to be done to obtain the structure in real space. To receive information on the atomic structure of the sample surface and potential adsorbates a so-called I-V curve analysis has to be performed.

I-V curves are intensity-voltage curves, which are obtained by collecting the LEED images with a CCD camera as a function of the primary electron beam acceleration voltage. At each step - usually every 2eV - two pictures are recorded and averaged to increase the signal to noise ratio. The pictures are analyzed off-line after the measurements.
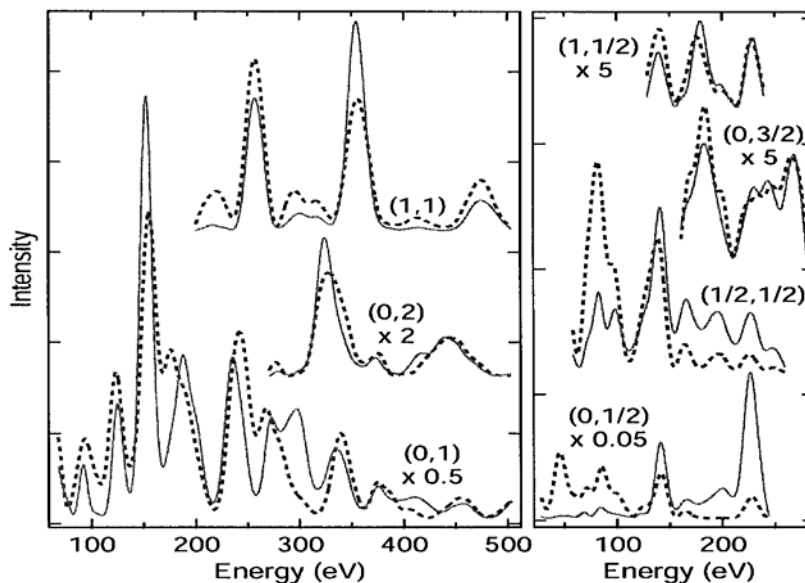

Fig.3: Comparison of experimentally (solid) and theoretically determined (dashed) I-V curves found as the best agreement for sulfur adsorbed on Co(0001). [Publ. VII]

To get information on the exact position of the atoms, trial structures have to be developed and appending I–V curves by computer simulation ascertained. These are then compared to the experimentally obtained curves. The model structure with the best achievable agreement between measured and calculated curves is further optimized by fitting all remaining parameters. An example for experimentally and computationally obtained I-V curves can be found in fig 3.

The quality of agreement of the two sets of I-V curves - the experimental and the calculated ones - is estimated by a reliability factor. The so-called Pendry R-factor is the most common one [16]. It is sensitive to the peak positions on the energy scale, but less sensitive to the absolute intensities, as these are influenced by processes like thermal vibration, inelastic loss or data collection related factors. By definition, an R-factor of 0 corresponds to perfect agreement while 1 stands for completely uncorrelated sets of curves. In a simple adsorption structure an R-factor of about 0.25 is considered to be good. With this procedure the exact location of adsorbed atoms or molecules can be determined [16-18].

2.6 Work Function (Φ) Measurements

The electron density at the surface is spilled out in the vacuum resulting in surface dipole layer. Due to this dipole layer a surface potential exists, which has to be overcome by a photoelectron to be able to leave the sample. As the spill out effect changes with the surface structure, different surface orientations of the same material exhibit different work functions. The dipole layer is also affected by adsorbates as they contribute additionally to the dipole layer, which explains why the work function changes with the adsorbate.

The work function (Φ) can be determined by measuring the high binding energy cutoff region of the XPS spectrum [19-23]. The change in the work function (ΔΦ) is directly reflected in the shift of the high binding energy cutoff edge. Fig 4 shows the high binding energy cutoff edge of clean Co(0001) and its shift due to adsorption of benzene and subsequently carbon monoxide. For clean Co(0001) the high binding energy edge

position is around 1248.05eV corresponding to a work function of about 5.55eV. Exposure to benzene shifts the edge to higher binding energies resulting in a binding energy edge about 1249.4eV and a reduction in the work function of about -1.3eV. With post-adsorbed CO a large number of benzene molecules desorb resulting in an increase in the work function to an absolute value of about 4.8eV.
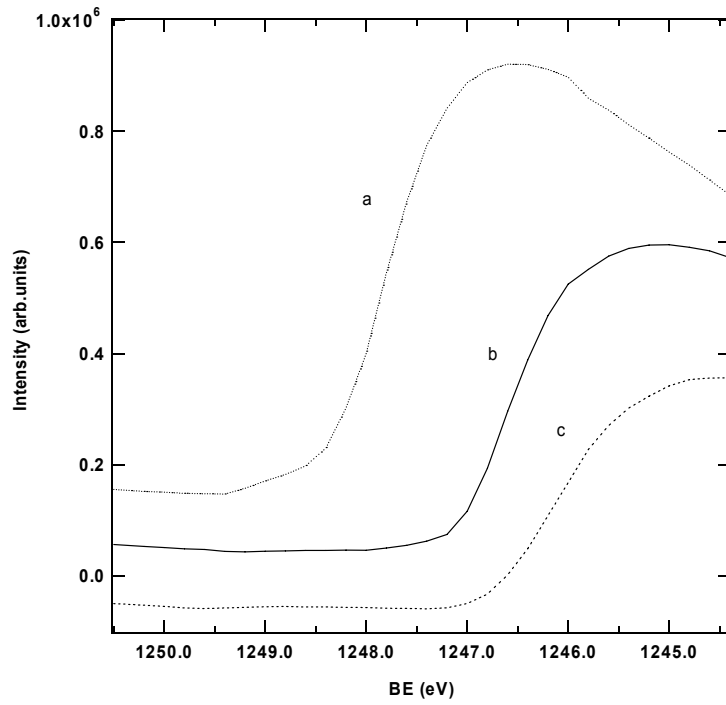

Fig. 4: High binding energy cutoff measured by XPS. Spectrum b has been obtained for a clean Co(0001) surface. Spectrum a is shifted compared to b towards higher binding energy due to adsorption of 14L of benzene. Spectrum c has been measured after the sample from spectrum a has been exposed to 66L of carbon monoxide.

3 Adsorbates on Co(0001)

3.1 Adsorption of Single Species

3.1.1 Deuterium

Hydrogen, an important molecule in many catalytic processes, is a challenging subject in surface science [24]. The main reasons for this complexity are the high mobility of hydrogen and the difficult and restricted measurement possibilities for hydrogen, e.g. AES (Auger electron spectroscopy) and XPS are unable to detect hydrogen due to its one-electron structure.

Deuterium was chosen as substitute for hydrogen to ensure that measurement signals were not altered by background hydrogen. The adsorption studies of deuterium were performed at two temperatures, 180K and 320K.

Results at these temperatures showed, that the adsorption of deuterium is not an activated process. An increase in the adsorption temperature led to a decrease in the total amount of adsorbed deuterium (fig. 5). A saturation value of about 0.27ML was reached for sample temperatures below 250K. Our LEED measurements confirm this finding by showing a (2x2) pattern – equivalent to coverage of 0.25ML – at 180K.
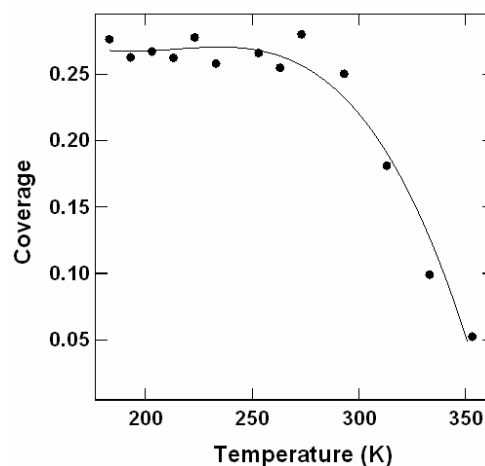

Fig.5: TDS yield of 200L of D_2 versus adsorption temperature. 200L corresponds to a value above the saturation limit. [Publ. I]

With both adsorption temperatures only one second-order desorption peak was found, exhibiting the characteristic symmetric peak shape and a peak shift to lower temperatures with increasing coverage. Deuterium desorption was found to start around 300K. The activation energy of desorption was calculated with the Redhead method [13] to be about 33kJ/mol, which is in agreement with values found for hydrogen desorption from polycrystalline Pt (18-33 kJ/mol) and Ru(0001) with 46kJ/mol [25,26].

WF measurements indicate that deuterium acts as an electron acceptor on Co(0001), as the WF increases with increasing coverage. At saturation level an increase of +200meV is found.

3.1.2 Methanol

Methanol - as a supplier for gaseous CO and H_2 – is a promising candidate for environmental friendly automobile fuel. Methanol adsorbed on a pure cobalt surface serves as a model for the development of cobalt-based catalysts in fuel cells.

The Co(0001) sample was exposed to 20L of methanol at 165K, leading to a saturation coverage of about 0.12ML. Methanol adsorbed by OH-bond scission as methoxide on Co(0001). WF measurements rule out the possibility of a completely dissociative adsorption as CO and hydrogen: The change in the work function after methanol saturation exposure was -1.1eV. A comparable amount of CO and hydrogen would increase the work function by +0.6eV.

During TDS a small amount of molecular methanol desorbed, while the majority of methoxide decomposed to CO and hydrogen (fig. 6). CO and H_2 desorbed molecularly from the surface, leaving a clean surface behind. CO-bond scission was not found. As no other decomposition products were produced, Co(0001) seemed to be an extremely effective methanol-decomposition catalyst.
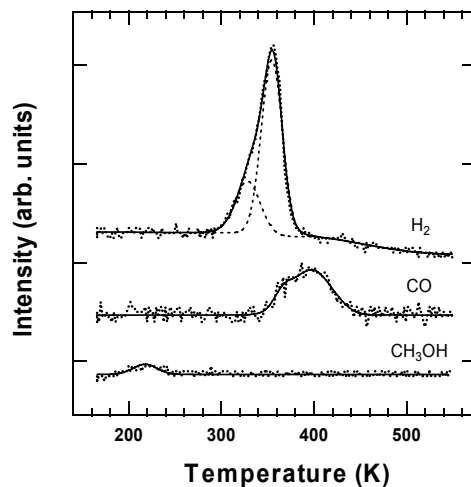
Fig. 6: TDS results after exposure to 20L of methanol. The doted lines show the experimental signals, while the solid lines represent the fitted values. The dashed lines represent the two components of the hydrogen signal. [Publ. II]

The TDS signal of hydrogen consisted of two peaks with a ratio of 1:3 as seen in fig. 6. We claimed that the smaller peak originates from OH-bond scission while the rest originate from the dehydrogenation of methoxide. The temperature values for desorption fit well to the values for desorption of CO and H_2 from clean Co(0001). The activation energies were calculated by the Redhead method and resulted in 33kJ/mol for hydrogen and 110kJ/mol for carbon monoxide.
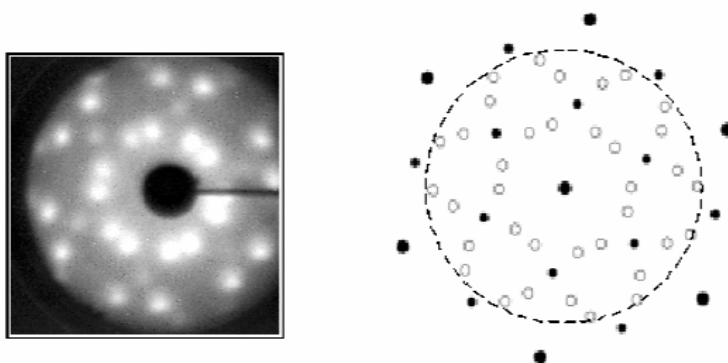

Fig. 7: The original and schematic LEED pattern showing the p(2x2) structure from CO and the $(\sqrt{7}\times\sqrt{7})19.1°$ structure originating from H_2. The pattern was recorded at 160K with an incident energy of 67eV. In the schematic drawing, the area inside the circle reflects the exact pattern seen with the experimentally obtained photo. The big filled circles ● are used for the cobalt substrate, • is representing the (2x2) phase and ○ the $(\sqrt{7}\times\sqrt{7})19.1°$ structure. [Publ. II]

The LEED pattern showed a surprising result. As seen in fig. 7, it consisted of a mixture of a p(2x2) and a ($\sqrt{7}$ x $\sqrt{7}$)19.1° structure. Heating caused the latter structure to disappear, while the (2x2) pattern was still observable when only substantial amounts of CO were found on the surface. A (2x2) structure had never been found for CO adsorption on Co(0001) before. A similar discovery was made by Hrbek et al. who obtained a (2x2) structure during studies of methanol on Ru(0001). For this system no CO induced (2x2) structure could be found either [27].

3.1.3 Benzene

Benzene is often used as a model molecule for aromatic molecules, as it is the simplest one of the family of aromatics.

Fig. 8 shows the p($\sqrt{7}$ x $\sqrt{7}$) structure which is obtained for high exposures and maximum adsorption temperatures up to 220K. The saturation exposure was easily reached by dosing 50L of benzene. This structure is equivalent to a nominal coverage of 0.143ML.

The change in the WF was followed for the adsorption of benzene at 160K. The work function changed to lower values for the adsorption of benzene. A minimum of -1.3eV is reached at saturation, leading to a total WF of 4.25eV.
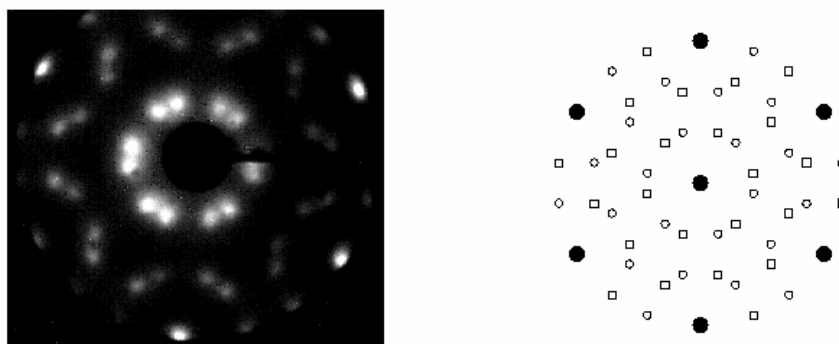

Fig. 8: ($\sqrt{7}$ x $\sqrt{7}$) LEED pattern of Co(0001) exposed to benzene at 220K. The picture on the right depicts the schematic pattern. [Publ. III]
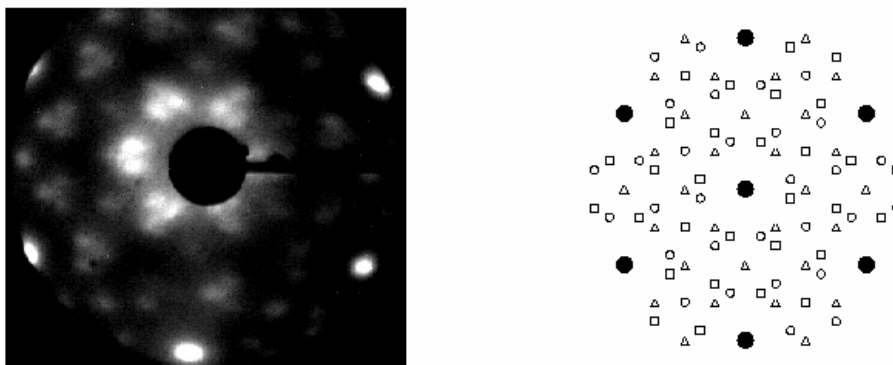
Fig. 9: LEED pattern obtained after adsorbing C_6H_6 on Co(0001) at RT. The pattern on the right shows the schematic drawing of the $c(2\sqrt{3} \times 4)$ structure. [Publ. III]

The cobalt sample was also exposed to benzene at 300K. Here an exposure of 30L was sufficient to saturate the sample surface. For these conditions a $c(2\sqrt{3} \times 4)$ LEED structure was obtained as shown in fig. 9. With this structure the saturation coverage was 0.125 ML.

TDS showed desorption of hydrogen molecules and a negligible amount of benzene. The variation in the TDS signal of H_2 with the amount of adsorbed benzene at 300K is shown in fig. 10. No other desorption products - like hydrocarbon fragments - were recorded. Benzene seemed to partially decompose during heating. By comparing the amount of desorbing hydrogen to the amount of adsorbed benzene, we found that, only one out of six hydrogen atoms of a benzene molecule desorbs. While the hydrogen combined and desorbed, the hydrocarbon fragment - most likely C_6H_5 - stayed adsorbed on the Co(0001) surface.

As the TDS spectra exhibited a first order desorption, the desorption-limiting step was suggested to be the decomposition of the benzene molecule. The activation energy of desorption was calculated to be about 102kJ/mol, showing almost the same value as the dehydrogenation of benzene on Co(10-10) [28].
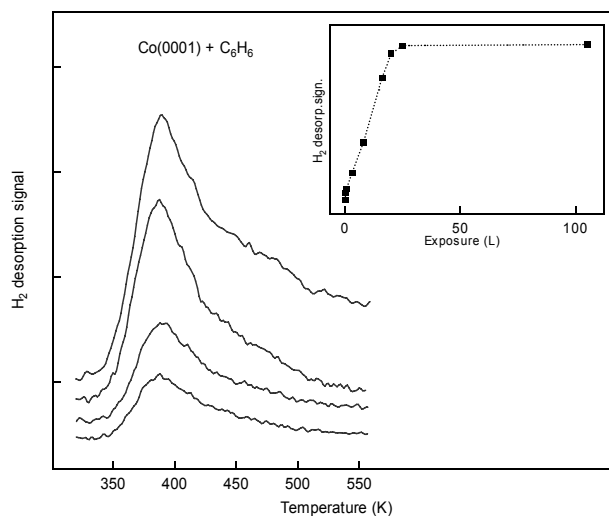
Fig. 10: TDS signal of H_2 originating from partly dissociated benzene. The exposure temperature was 300K and the benzene exposure was varied between 4 and 25L relating to the spectra from bottom to top. The absolute value of the H_2 desorption signal versus the benzene exposure is graphically displayed in the inset. The line is drawn to guide the eye. [Publ. III]

A Tensor LEED and DFT study focusing on the benzene $(\sqrt{7} \times \sqrt{7})$R19.1° structure was performed to obtain the exact adsorption structure. The $(\sqrt{7} \times \sqrt{7})$R19.1° was given preference as the low adsorption temperature is favorable with LEED studies. For this purpose, the cobalt single crystal was exposed to 50L of benzene at 220K. The I-V data were recorded after cooling the sample to about 170K. 170K corresponds to the lowest temperature possible with our apparatus, thereby ensuring a steady temperature of the sample during the whole LEED I-V measurement. I-V measurements were done at normal incidence between 20-500eV, with energy steps of 2eV. The cumulative energy range was 1470eV.

Fig. 11 shows in the upper right corner the beams used for this calculation. The I-V data consist of 9 beams, as the (2/7, 8/7) and (9/7, 1/7) beams overlapped and were therefore averaged. Each beam was corrected by subtracting a user-chosen exponentially-increasing background. The exponential form has its origin in the increasing intensity of the background due to diffraction spots approaching each other with increasing beam energy.
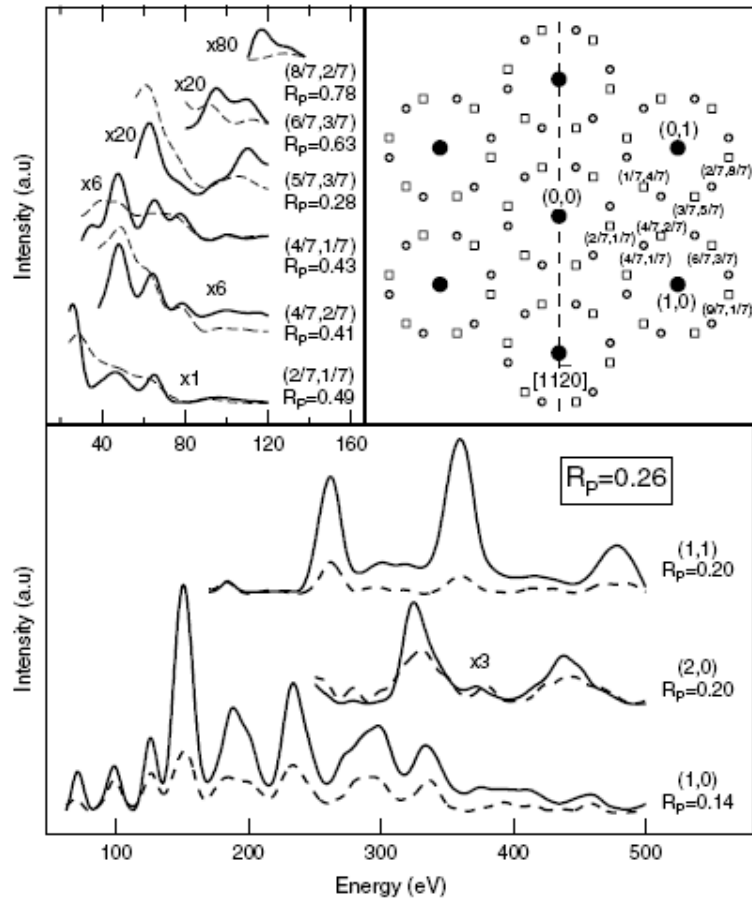
Fig. 11: At the top right the beams used for the calculation are indexed and the two domains illustrated by different signs (O, □). At the top left the I-V curves for the fractional-order beams and the corresponding reliability factors are shown. At the bottom the I-V curves and P_R factors of the integral spots can be seen. The experimental curves are solid and the theoretical curves dashed. [Publ. IV]

For the density functional theory calculations a slab of five atomic layers thickness, 12Å vacuum and one benzene molecule in the primitive ($\sqrt{7}$ x $\sqrt{7}$)R19.1° unit cell was used.

Fig. 12 shows the eight preliminary configurations, which were chosen in the beginning of the research. As adsorption sites top, hcp, fcc and bridge were considered. Additionally two orientations of the benzene molecule were considered: A and B. Within A two C-C bonds were aligned with the [1-100] direction, while within B they were aligned with the [11-20] direction. The degree of agreement between theory and experiment was tested using the Pendry R-factor. The structure agreeing best to the experimental I-V curves was the hcp A structure with a Pendry R-factor of 0.26 as displayed in Fig. 13.
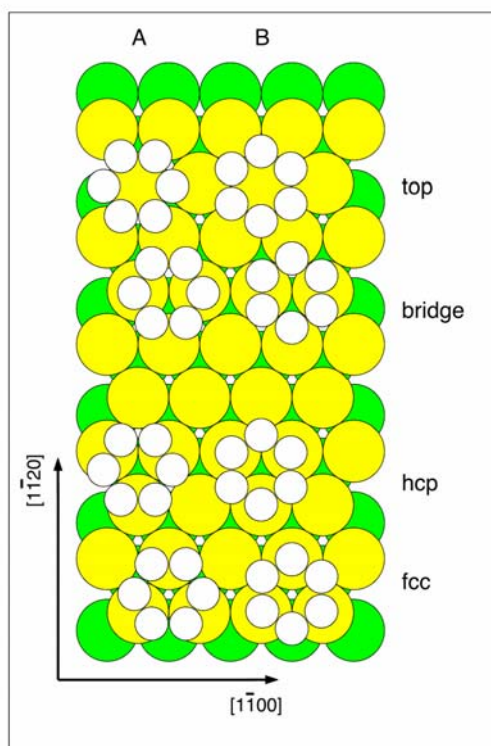
Fig. 12: All high-symmetry adsorption sites which were considered for the I-V calculation. The carbon atoms of the benzene molecule and the top cobalt layers are shown. [Publ. IV]

Practically the adsorbed benzene molecule experienced no major changes compared to the gas phase benzene: The carbon ring exhibited a negligible buckling between two inequivalent carbon atoms. The hydrogen-carbon bonds were slightly expanded with the bond length of 1.1 ± 0.2Å compared to 1.08Å in the gas phase. The center of mass of the hydrogen atoms is located 0.3 ± 0.2Å above the center of mass of the carbon ring.

The substrate structure wasaltered due to the benzene adsorption, as the second interlayer spacing is found to expand by 3% while the third interlayer spacing was contracted by 3%. Though the first interlayer spacing remained similar to the bulk value, a strong buckling was found in the first layer. Especially the substrate atoms right below the benzene ring were displaced by about 0.09 ± 0.06Å towards the benzene ring.
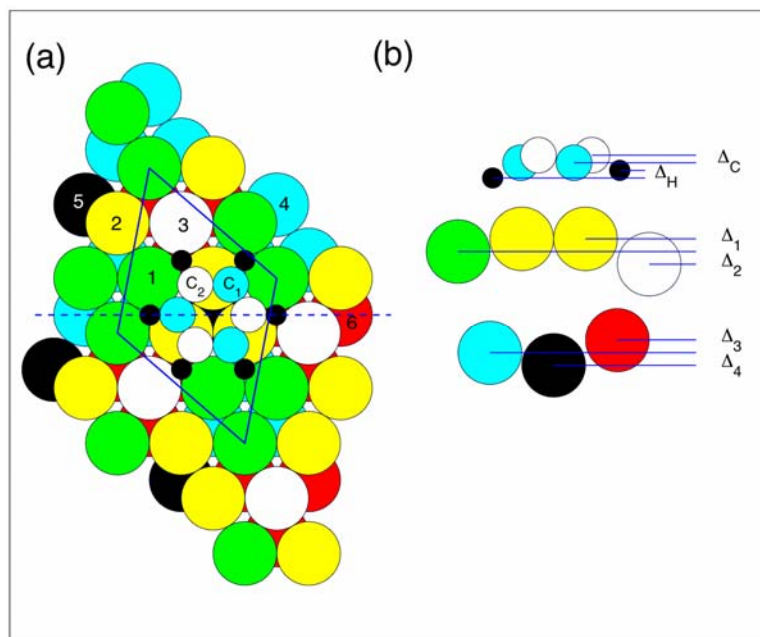
Fig. 13: Top and side view of the structure showing the best agreement in the I-V calculation with the experimentally obtained I-V curves. [Publ. IV]

DFT calculations gave a slightly different picture. The benzene ring seemed to be slightly expanded and large buckling of 0.19Å of the first cobalt layer was found. A difference in the buckling values has been found earlier with Ru(0001), Ni(111) and Pt(111). In all cases the experimentally derived buckling values are smaller than the DFT values [29-32].

The DFT calculations showed a reduction in the WF by 1.67eV, while the experimental decrease was -1.3eV. The order of magnitude seems to correlate quite well and DFT calculations typically underestimate the absolute WF value. The absolute values differed substantially from each other, as the experimental value for the clean cobalt (0001) has been assigned to be 5.55eV, while the DFT calculation gave a value of 5.05eV.

The DFT calculations left the question of the preferred adsorption site open as the hcp A and the fcc A gave practically identical adsorption energies. Due to the Tensor-LEED result the hcp A site is expected to be the favorable adsorption site.

3.1.4 LEED and DFT Investigation on (2x2)-S

Sulfur can act as a strong poison in catalytic processes. Moreover, sulfate-containing components are frequently found, e.g. in crude oil, and have to be removed not only out of process-related reasons but also due to environmental restrictions before further processing.

We found that the saturation coverage of sulfur at room temperature corresponds to 1/3 ML. With decreasing adsorption temperature the saturation coverage decreases. At 220 K the saturation layer exhibits in LEED a very stable (2x2) structure corresponding to quarter ML coverage.

The (2x2) structure has been found with several close-packed surfaces. Ru(0001), Re(0001), Ni(111), Pt(111) as well as Co(0001) exhibit this sulfur pattern [33-37]. Earlier results show that the favorite adsorption site for sulfur on hcp metals is the hcp site. Then again on fcc metals, the fcc site is the preferred adsorption site.

The actual adsorption geometry of sulfur on Co(0001) was calculated in our study by means of experimentally obtained LEED I-V curves as well as Tensor LEED and DFT calculations. The LEED measurements were performed at 220K. Sulfur was deposited on the sample surface by exposing the clean cobalt sample at 220K to hydrogen sulfide. After flashing the sample to 650K the hydrogen desorbs and the surface is left behind with an ordered sulfur layer.

Each I-V curve was suitably corrected by subtracting an exponentially increasing background. Additionally symmetrically equivalent beams were averaged in order to increase the signal to noise ratio. The theoretical I-V curves were calculated in a range of 25-510eV with the Tensor LEED package by Barbieri and Van Hove [38]. Comparison between calculated and experimental I-V curves was done using the Pendry R-factor [16].

In the LEED I-V calculation fcc, hcp, bridge and top sites were considered. The fcc site yielded a minimum Pendry R-factor of 0.159. The distance between the sulfur and the topmost cobalt layer is 1.59 ± 0.06Å with an S-Co distance of 2.10 ± 0.1Å. The first cobalt layer relaxed slightly outwards and reconstructed due to sulfur adsorption. In the

reconstruction the three nearest Co atoms beneath the sulfur atom move symmetrically by 0.05 ± 0.09Å within the topmost layer. Fig. 3 shows the experimentally obtained I-V as well as the calculated I-V curves for the favored adsorption site.

The adsorption geometry of one S atom in the 2 x 2 unit cell was additionally determined by DFT calculations, using a slab of seven atomic cobalt layers and a vacuum of about 10Å. The DFT calculations suggest that the fcc and the hcp site are the favorable adsorption sites as both sites exhibit the smallest adsorption energies with a negligible difference of 0.02eV between them. The distance between sulfur and the first cobalt layer is estimated to be 1.61Å with an S-Co distance of 2.16Å. Fig. 14 illustrates the schematic structure of this adsorption structure.
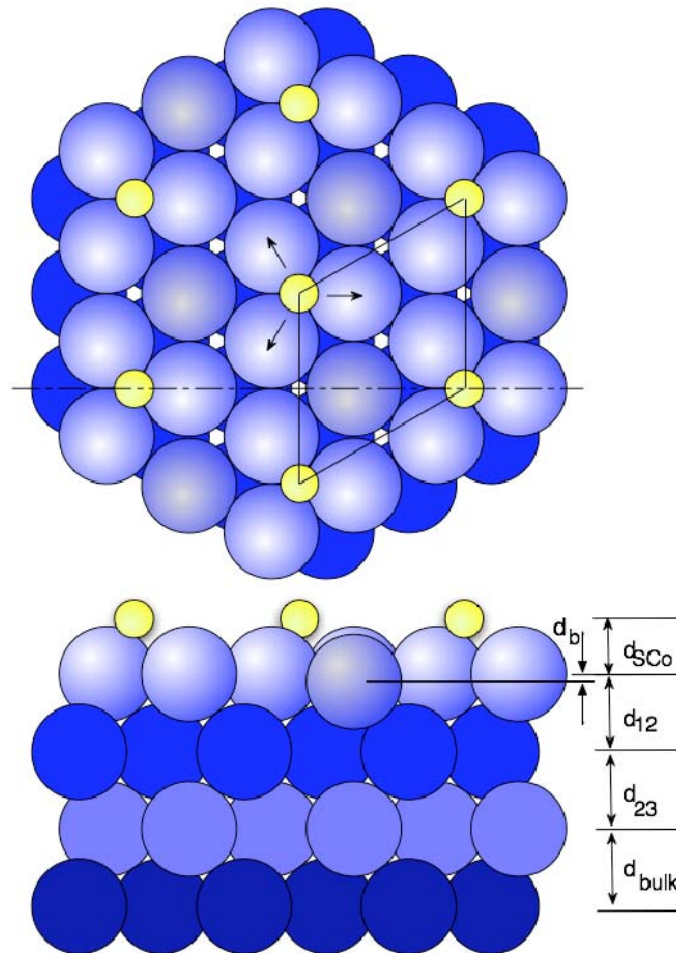

Fig. 14: Top and side view of the computationally determined structure which shows the best agreement with the experimentally obtained curves. [Publ. IV]

The trend found in the literature for the (2x2)-S system, where the sulfur adsorpotion site reflects the bulk structure is contradicted in this study. The theoretical calculations for the (2x2)-S system are not unambiguously in favor of hcp being the preferred adsorption site on Co(0001). DFT favors the fcc site, but the energy difference between the fcc and hcp sites is with 0.02eV very small. The LEED I-V analysis results in the fcc site having the lowest Pendry R-factor and is therefore the favorite adsorption site.

3.2 Coadsorption

3.2.1 Deuterium and Carbon Monoxide

CO acts as an electron acceptor on transition metals. Together with alkali metals attractive interaction leading to mutual stabilisation was found earlier [39]. In principle the same sort of behavior could be suggested with the system H/CO, as hydrogen belongs to the same group in the periodic system as alkali metals. Nevertheless, pure hydrogen adsorption showed that hydrogen acts as an electron acceptor on Co(0001). Therefore coadsorption of deuterium with carbon monoxide leads to a repulsive interaction between the coadsorbed species. This fact is clearly seen in the TDS spectra of fig. 15. Increasing amounts of CO lead to a shift in the peak maximum temperature to lower temperatures as well as a decrease in the deuterium yield. This decrease saturates at 50% of the initial deuterium yield.

Deuterium itself seems to have no profound impact on the CO adsorption, with one exception. The $(\sqrt{7/3} \times \sqrt{7/3})R10.9°$ pattern of CO could not be obtained. As this structure is suggested to be based on mutual stabilization between the CO molecules, deuterium seems to influence this interaction. Otherwise no changes in the CO behavior compared to pure CO adsorption is found. The amount of adsorbed CO corresponds to the amount found for pure CO adsorption. Also the decrease in the peak maximum temperature of CO is known from studies of pure CO. The difference in the impact of the coadsorption of the individual species - CO versus D_2 - is explained by the high mobility of deuterium on the Co(0001) surface.
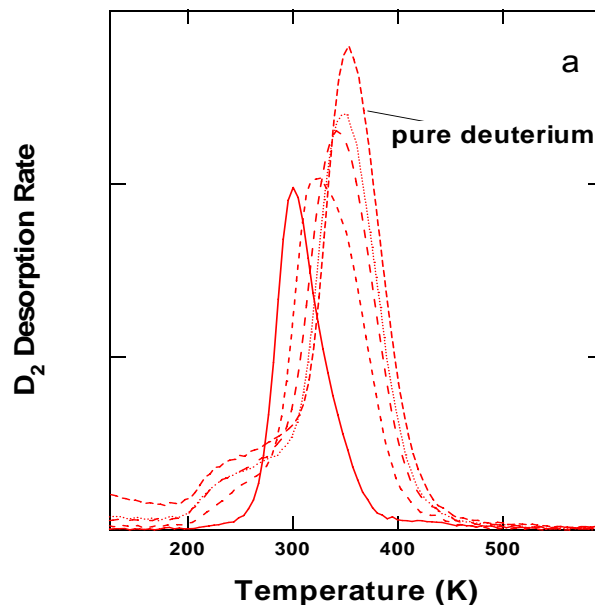
Fig.15: TDS yield of 200L of D_2 versus adsorption temperature after various CO exposures between 0-5L. With increasing amount of CO the desorption peak of deuterium shifts to lower temperature and simultaneously the desorption yield is reduced. [Publ. I]

3.2.2 Deuterium and Sulfur

The sulfur covered cobalt surface was exposed to 200L of deuterium. The value of 200L was chosen to ensure saturation condition. TDS showed that the only gaseous product evolved was D_2. Sulfur pre-adsorption seems to cause the deuterium atoms to populate energetically less favorable sites as the spectra show that an increasing amount of pre-adsorbed sulfur leads to a downwards shift in the peak maximum temperature of deuterium. While the peak maximum temperature for deuterium on clean cobalt is found around 375K, the co-adsorption of 0.25ML with sulfur leads to a decrease in the peak maximum temperature by 85K. As even small amounts of sulfur strongly suppress the adsorption of deuterium, no measurable changes in the WF were found after deuterium exposure.

Furthermore, deuterium adsorption is reduced by a factor of three with increasing sulfur coverage from 0ML to 0.25ML. A further increase in the sulfur coverage results in the complete prevention of deuterium adsorption. The reason for this is probably a purely site-blocking effect, as the inset of fig. 16 exhibits a linear dependence of the deuterium

coverage on the sulfur precoverage. Such a linear dependence is generally found with direct local site blocking.
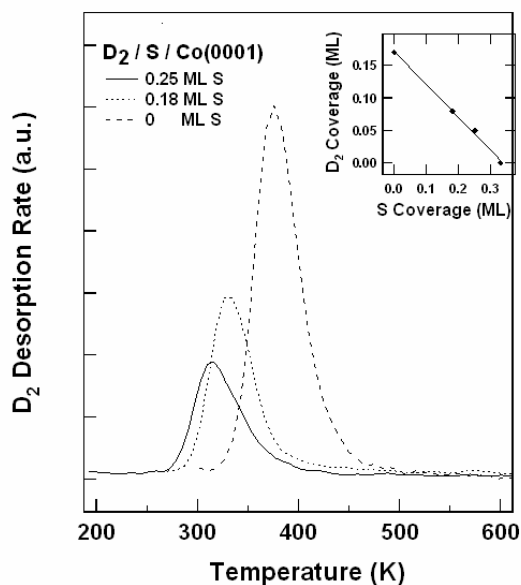

Fig. 16: TDS signal for 200L of deuterium for sulfur-covered Co(0001). The exposure took place at room temperature. The inset shows that the desorption yield of D_2 decreases linearly with increasing amount of sulfur. [Publ. I]

While with pure deuterium adsorption the LEED pattern consists of a faint (2x2) structure, post-adsorption of deuterium on the sulfur-covered surface did not give rise to additional LEED spots. This behavior indicates that no long-range order of deuterium on a sulfur-covered Co(0001) surface exists.

The results show impressively that sulfur is a strong poison to the hydrogen adsorption and to the cobalt catalyst in general, as sulfur cannot be easily removed by heating.

3.2.3 Sulfur and Carbon Monoxide

Carbon monoxide is an extensively studied molecule, which takes part in various heterogeneous catalytic processes. CO is known to exhibit on Co(0001) a saturation coverage of about 0.56 ± 0.02ML at 180K with CO molecules occupying top as well as hollow sites [40]. However, sulfur is frequently found as an unwanted component in

CO-containing reactants, like gasified biomass or methanol. Hydrodesulphurization over CoMo catalysts is here an important industrial application.

We investigated the behavior of pre-adsorbed sulfur on the adsorption of CO at 180K. For this purpose sulfur coverages of 0-0.25ML were chosen as basis.

LEED showed two structures upon coadsorption of 0.25ML of S depending on the amount of post-adsorbed CO. Up to 2L of CO the p(2x2) structure, corresponding to sulfur saturation was detected, while with increased CO exposure the $(2\sqrt{3} \times 2\sqrt{3})R30°$ was seen.

Pre-adsorbed sulfur partially blocked the adsorption of CO. This resulted - at sulfur saturation – in blocking of 1.2 CO sites by one sulfur atom. This behavior led to a decrease in the C1s spectra with increasing sulfur coverage. For 1L of CO, the one-peak-C1s spectrum changes to a two-peak spectrum with increasing amount of sulfur. This two-peak spectrum is known from high coverages of CO. The C1s peaks are found at 286.4eV and 285.8eV as shown in fig. 17. The latter corresponds to adsorption on less favorable bridge or hollow sites, while the higher binding energy site resembles the on-top adsorption site.
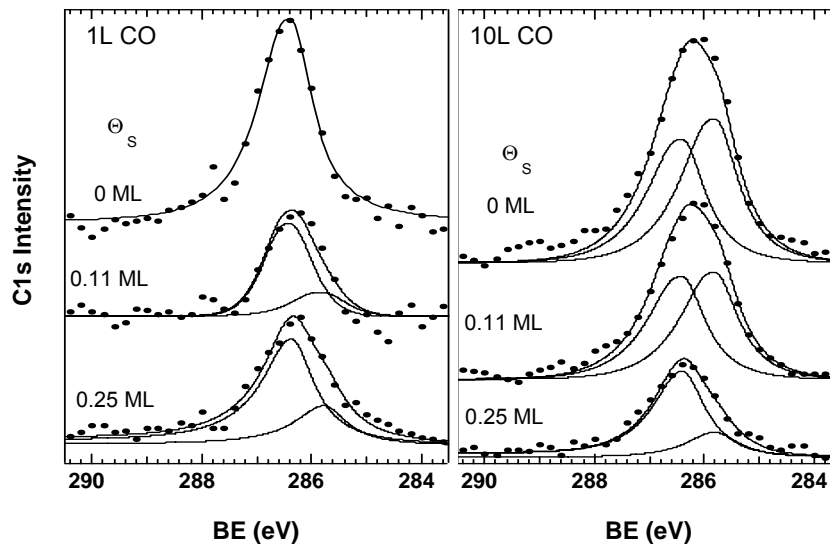

Fig. 17: XPS C1s spectra for exposure of 1 and 10L of CO. The Co(0001) sample was precovered with 0, 0.11 and 0.25L of sulfur. The data in the left figure are multiplied by a factor of two. The figures contain additionally the fitted components representing two different adsorption sites of CO. [Publ. VI]

In the case of a small CO exposure, increasing sulfur precoverage leads to an increased amount of CO adsorbing on hollow sites. With 10L of CO the on-top adsorbed CO molecules are less influenced by sulfur than the CO adsorbed on hollow sites (fig. 18). Here CO adsorption on hollow sites is greatly reduced up to the limit of approximately the same amount of available hollow sites for CO as in the case of 1L of CO.

Blocking of CO adsorption was also seen from the WF results, as CO saturation on a clean surface resulted in a WF change of 1.2eV. With increasing amount of sulfur this value decreased and resulted in a value of 0.5eV for CO on a sulfur saturated surface (fig. 18).
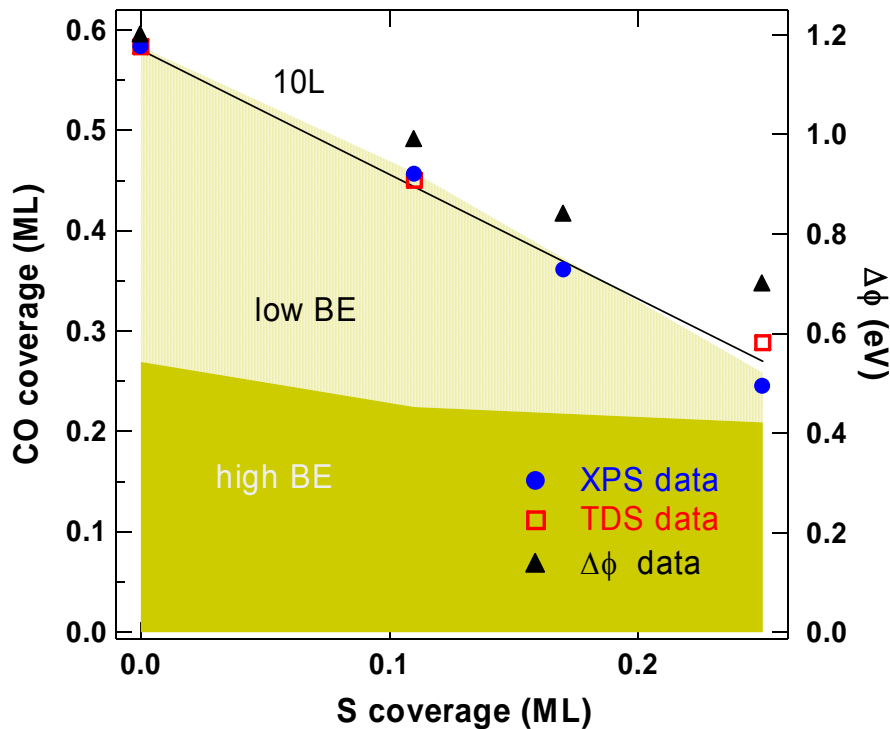

Fig. 18: Amount of adsorbed CO versus sulfur precoverage for a CO exposure of 10L. The solid circles represent XPS data, the open sqares TDS data and the triangles WF data. The WF data represent solely the data obtained from CO adsorption. [Publ. VI]

TDS data of 10L of CO coadsorbed with various amounts of sulfur (fig. 19) show the tremendous power of sulfur on the bonding strength of CO. The two TDS peaks of CO moved to lower temperatures with increasing amount of sulfur. The low temperature peak - at pure CO adsorption around 280K - moved to 240K. The high temperature peak shifted about 85K to 315K. This influence is directly seen in the activation energy

of desorption of CO, changing from 113kJ/mol to 88kJ/mol for pre-saturated sulfur for the high temperature CO peak and from 78kJ/mol to 66kJ/mol for the low temperature peak. We claim that S atoms attract charge from the substrate and therewith reduce the back donation of electrons from cobalt to CO, leading to the decrease in the activation energy of desorption.
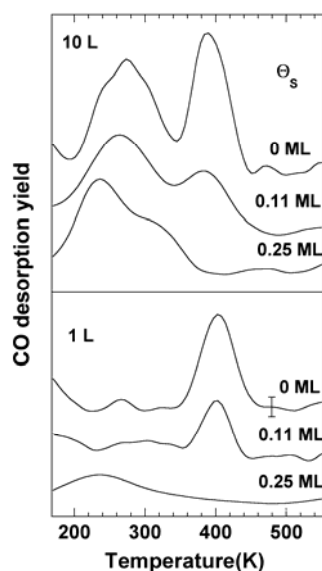

Fig. 19: Smoothed TDS data of CO for 1 and 10 L of CO and three different sulfur precoverages. [Publ. VI]

Our results show that sulfur is a powerful poison for CO containing catalytic processes on cobalt. Sulfur does neither promote the CO dissociation nor its disproportionation, but greatly reduces the amount of CO adsorbed as well as its bonding strength. Additionally sulfur stays adsorbed on the cobalt during moderate heating, making it more difficult to get rid of the negatively affecting sulfur.

3.2.4 Benzene and Carbon Monoxide

Coadsorption of C_6H_6 and CO is an interesting research topic as CO is found in a variety of catalytic processes, either as desired reactant or unwanted contamination and benzene serves as a model for aromatic molecules. As benzene acts as an electron donor, while carbon monoxide is known as acceptor of metal electrons in its $2\pi^*$ orbital, a strong interrelationship would be presumed.
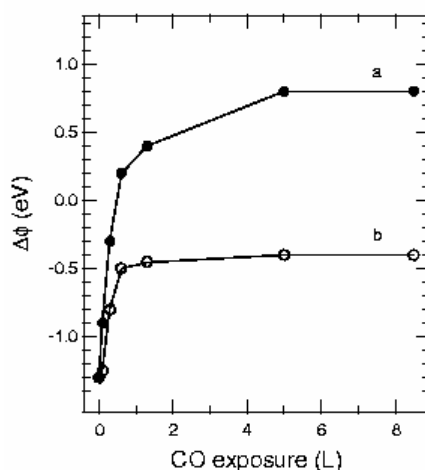
Fig. 20: WF change (ΔΦ) versus CO preadsorption. The amount of benzene was kept at 14L and the exposure temperature at 180K. (a) shows the change in the WF before and (b) after TDS. [Publ. V]

As the obtained results of our study show only minor differences for the reversion in the exposure sequence, we show here the results for CO preadsorption. The adsorption of 14L of benzene on a clean Co(0001) surface leads to a decrease of the WF of -1.3eV. With increasing amount of preadsorbed CO this value changes and saturates at +0.8eV for CO saturation. The change in the WF due to the coadsorption of CO and C_6H_6 is displayed in fig. 20.

The preadsorbed CO decreases the amount of adsorbed benzene by partial site-blocking to about one-third of the saturation level on clean cobalt. Carbon monoxide itself is not influenced by the post adsorption of benzene (fig. 21).
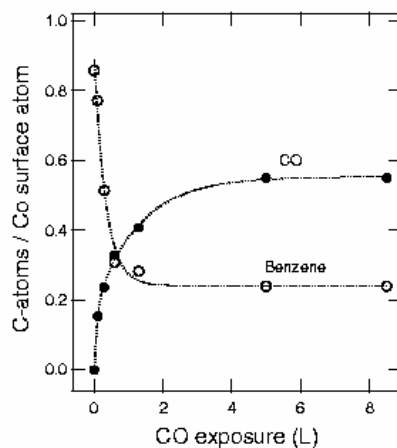

Fig. 21: Carbon atom coverage as a function of preadsorbed carbon monoxide. The benzene exposure was kept constant with 14L. [Publ. V]
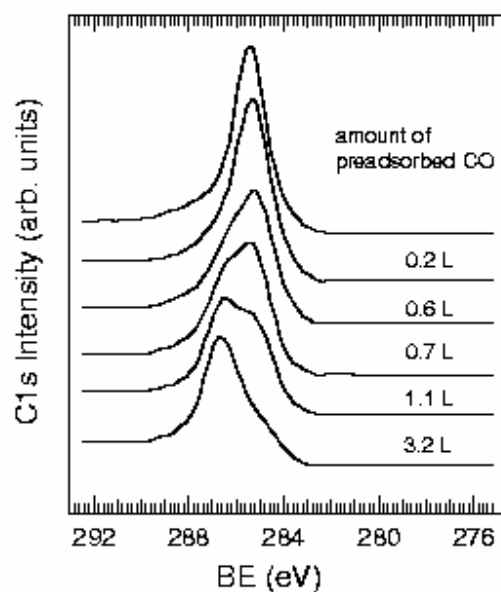
Fig. 22: XPS spectra of carbon monoxide and benzene coadsorption. The figure displays the change in the photoelectron spectra with increasing amount of pre-adsorbed CO. [Publ. V]

With XPS a single C1s peak at 285.1eV was obtained for pure benzene exposure (fig. 22). With pre-adsorbed CO a second peak at 286.2eV appeared in the spectrum; corresponding to on-top site adsorption. Above 1.1L of pre-adsorbed CO this peak became dominant in the spectrum. While the C1s peak of CO stayed constant at 285.1eV, the binding energy of benzene decreased with increasing amount of pre-adsorbed CO, leading to a BE of 284.5eV for benzene at CO saturation level.

Thermal desorption measurements traced CO, H_2 and a negligible amount of benzene. No other desorption products were found. The CO desorption was molecular and no CO-bond scission was found. The temperature maxima of hydrogen and CO were the same as for adsorption of the single components. These results make it clear that the attraction between carbon monoxide and benzene is surprisingly small.

From our former study we know, that benzene adsorbs at the hcp site. With carbon monoxide populating on-top sites there are hcp sites for benzene available in the $(\sqrt{7} \times \sqrt{7})$R19.1° coadsorption structure (fig. 23). We have shown that with an increasing amount of CO, the CO-CO interaction becomes dominant, the $(\sqrt{7} \times \sqrt{7})$R19.1° structure disappears and the carbon monoxide related structures appear. When this occurs, the benzene molecules are getting displaced and even

change their orientation on the surface or might even change their adsorption from flat to tilted.
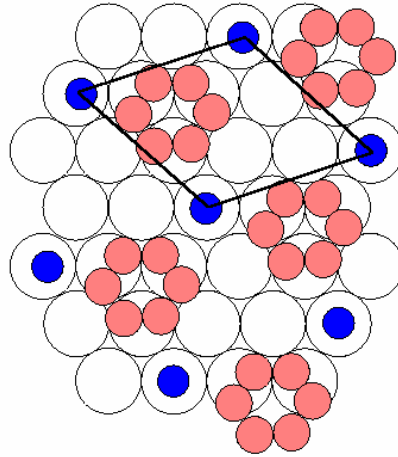

Fig. 23: Schematic drawing of the proposed $(\sqrt{7}\times\sqrt{7})R19.1°\text{-}C_6H_6+CO$ structure. The adsorption sites are based on the adsorption of pure CO and pure C_6H_6 on Co(0001). [Publ. V]

4 Summary and References

Our results show that hydrogen adsorption is a non-activated process resulting in atomic hydrogen on the surface. Coadsorbed CO decreases the hydrogen adsorption to 50% of the value obtained for pure hydrogen adsorption. Besides, a drop in the activation energy for desorption is found. Preadsorbed sulfur is also leading to a decrease in the hydrogen bonding, but exhibits a greater influence as it completely inhibits hydrogen adsorption close to the sulfur saturation coverage. Sulfur does not leave the catalyst by simple heating and therefore substantiates its status as catalyst poison.

The main component found after methanol exposure is methoxy. During heating methoxy decomposes solely to CO and hydrogen. Both components desorb from the surface with increased heating, leaving a clean catalyst behind.

Benzene adsorption on cobalt leads to a hydrocarbon fragment – most likely C_6H_5 – and adsorbed hydrogen. During heating hydrogen desorbs and the hydrocarbon fragment stays adsorbed. Dynamical LEED and DFT studies show that the adsorption site in the $(\sqrt{7} \times \sqrt{7})R19°$ adsorption structure of benzene is the hcp site.

Benzene adsorption is reduced by CO coadsorption. Whether CO is post- or preadsorbed, benzene adsorption is reduced to 30%. CO, H_2 and a negligible amount of benzene is found as desorption products. The great amount of benzene stays adsorbed at the catalyst surface.

Preadsorption of sulfur leads to partial blocking of CO. Due to sulfur carbon monoxide adsorbs also on less favorable sites. The influence of sulfur is also seen in the decrease in the activation energy for desorption. Nevertheless, sulfur does not facilitate CO bond scission.

LEED and DFT calculations of the S (2x2) structure show that sulfur adsorbs on the fcc hollow sites. This result is unexpected as commonly sulfur was found to adsorb on fcc site with fcc crystals and hcp site with hcp crystals.

References

[1] P.R. Taube and J.I. Rudenko, Die chemischen Elemente, Aulis Verlag Deubner & Co. (1968).

[2] N.N.Greenwood and A. Earnshaw, Chemistry of the elements, Pergamon Press (1989).

[3] DECHEMA (2004), Advances in catalyst technology are the motors of chemical processing [online], available at: URL: http://www.dechema.de/13___Catalysis-lang-en-site-dechemaneu.html (Accessed 29th November 2005).

[4] Natural Gas Supply Association (2004), Natural Gas – From Wellhead to Burner Tip [online], available at: URL: http://www.naturalgas.org/naturalgas/naturalgas.asp (Accessed 29th November 2005).

[5] J. Vaari, Doctoral Dissertation, Helsinki University of Technology (1995).

[6] R. Nix (2003), An Introduction to Surface Chemistry [online], available at: URL: http://www.chem.qmw.ac.uk/surfaces/scc/ (Accessed 29th November 2005).

[7] UK Surface Analysis Forum (2001), An Introduction to TPD, TDS and TPRS [online], available at: URL: http://www.uksaf.org/tech/tpd.html (Accessed 29th November 2005).

[8] G.A. Somorjai, Introduction to Surface Chemistry and Catalysis, John Wiley & Sons (1994).

[9] S.J. Garrett (2001), Introduction to Surface Analysis [online], available at: URL: http://www.cem.msu.edu/~cem924sg/LectureNotes.html (Accessed 29th November 2005).

[10] H. Lueth, Surfaces and Interfaces of solid materials, Springer-Verlag (1997).

[11] G. Attard and C. Barnes, Surfaces, Oxford University Press (1998).

[12] J.W. Niemantsverdriet, Spectroscopy in Catalysis, VCH (1995).

[13] P.A.Redhead, Vacuum **12** (1962) 203.

[14] D. Briggs and M.P. Seah, Practical Surface Analysis by Auger and X-ray Photoelectron Spectroscopy, John Wiley & Sons (1987).

[15] University of York (2003), Low Energy Electron Diffraction [online], available at: URL: http://www-users.york.ac.uk/~phys24/Pages/Techniques/LEED/ (Accessed 29th November 2005).

[16] J.B. Pendry, J. Phys. C.: Solid State Phys. **13** (1980) 937.

[17] Y.D. Kim, Doctoral Dissertation, FU Berlin (2000).

[18] H. Bubert and H. Jenett, Surface and Thin Film Analysis, Wiley-VCH (2002).

[19] C.R. Brundle and A.D. Baker, Electron Spectroscopy: Theory, Techniques and Applications (Volume 2), Academic Press (1981).

[20] J. Schwartz, E.L. Bruner, N. Koch, A. R. Span, S.L. Bernasek and A. Kahn, Synthetic Metals **138** (2003) 223.

[21] H. Ishii, K. Sugiyama, W. Ito and K. Seki, Av. Mater. **11** (1999) 605

[22] R.Schlaf, C.D. Merritt, L.A. Crisafulli and Z.H. Kafafi J.Appl.Phys. **86** (10) (1999) 5678.

[23] E.L. Bruner et al. J.Am.Chem.Soc **124** (2002) 3192.

[24] K. Christmann, Surf.Sci.Rep. **9 (**1988) 1.

[25] V.D. Thomas, J.W. Schwank and J.L. Gland, Surf. Sci. **501** (2002) 214.

[26] J.A. Schwarz Surf. Sci. **87** (1979) 525.

[27] J. Hrbek, R.A. dePaola, F.M. Hoffmann, J.Chem. Phys. **81** (1984) 2818.

[28] C.J. Barnes, M. Valden, M. Pessa, Surf. Rev. Lett. **7** (2000) 67.

[29] G. Held, M. Bessent, S. Titmuss and D.A. King, J. Chem. Phys. **105** (1996) 11305.

[30] F. Mittendorfer and J. Hafner, Surf. Sci. **472** (2001) 133.

[31] S. Yamagishi, S.J. Jenkins and D.A. King, J. Chem. Phys. **114** (2001) 5765.

[32] C. Morin, D. Simon and P.Sautet, J. Phys. Chem. B. **107** (2003) 2995.

[33] D. Juergens, G. Held and H. Pfnuer, Surf. Sci. **303** (1994) 77.

[34] A. Barbiere, D. Jentz, N. Materer, G. Held, J. Dunphy, D.F. Ogletree, P. Sautet, M. Salmeron, M.A.Van Hove, G.A. Somorjai, Surf. Sci. **312** (1994) 10.

[35] J. Luedecke, A.R.H.F. Ettema, S.M. Driver, G. Scragg, M. Kerkar, D.P. Woodruff, B.C.C. Cowie, R.G. Jones and S. Bastow, Surf. Sci. **366** (1996) 260.

[36] D.R. Warburton, P.L. Wincott, G. Thornton, F.M. Quinn and D. Norman, Surf. Sci. **211/212** (1989) 71.

[37] H.A. Yoon, N. Materer, M. Salmeron, M.A.Van Hove and G.A. Somorjai, Surf. Sci. **376** (1977) 254.

[38] K. Pussi, A. Barbieri and M.A. Van Hove, private communication.

[39] T. Vaara, Doctoral Dissertation, Helsinki University of Technology (1997).

[40] J. Lahtinen, J. Vaari and K. Kauraala, Surf. Sci. **418** (1998) 502.